Entropy **2015**, *17*, 4454-4484; doi:10.3390/e17064454

OPEN ACCESS
entropy
ISSN 1099-4300
www.mdpi.com/journal/entropy

Article

Modeling Soil Moisture Profiles in Irrigated Fields by the Principle of Maximum Entropy

Vikalp Mishra [1], Walter L. Ellenburg [1], Osama Z. Al-Hamdan [2], Josh Bruce [3] and James F. Cruise [1,*]

[1] Earth System Science Center, National Space Science and Technology Center, University of Alabama in Huntsville, 320 Sparkman Drive, Huntsville, Al 35805, USA; E-Mails: vikalp.mishra@nsstc.uah.edu (V.M.); lee.ellenburg@uah.edu (W.L.E.)

[2] Northwest Watershed Research Center, USDA Agricultural Research Service, 800 E. Park Blvd, Plaza IV, Suite 105, Boise, ID 83712, USA; E-Mail: Osama.Al-Hamdan@ars.usda.gov

[3] Department of Civil and Environmental Engineering, University of Alabama in Huntsville, 301 Sparkman Drive, Huntsville, AL 35899, USA; E-Mail: jgb0010@alumni.uah.edu

***** Author to whom correspondence should be addressed; E-Mail: james.cruise@nsstc.uah.edu; Tel.: +1-256-961-7659.

Academic Editor: Nathaniel A. Brunsell

Received: 26 April 2015 / Accepted: 18 June 2015 / Published: 23 June 2015

Abstract: Vertical soil moisture profiles based on the principle of maximum entropy (POME) were validated using field and model data and applied to guide an irrigation cycle over a maize field in north central Alabama (USA). The results demonstrate that a simple two-constraint entropy model under the assumption of a uniform initial soil moisture distribution can simulate most soil moisture profiles that occur in the particular soil and climate regime that prevails in the study area. The results of the irrigation simulation demonstrated that the POME model produced a very efficient irrigation strategy with minimal losses (about 1.9% of total applied water). However, the results for finely-textured (silty clay) soils were problematic in that some plant stress did develop due to insufficient applied water. Soil moisture states in these soils fell to around 31% of available moisture content, but only on the last day of the drying side of the irrigation cycle. Overall, the POME approach showed promise as a general strategy to guide irrigation in humid environments, such as the Southeastern United States.

Keywords: maximum entropy; soil moisture; irrigation efficiency

1. Introduction

Irrigation efficiency is a primary concern of irrigating farmers around the world. It is defined as the ratio of the amount of water beneficially used by the crop or its ecosystem to the volume of water applied minus the change in soil moisture storage [1]. Beneficial water use is the amount of water that is utilized for crop evapotranspiration (ET), soil evaporation for climate control, leaching to reduce soil salinity and water storage incorporated in the biomass [1,2]. Thus, to maximize irrigation efficiency, the goal is to only apply the amount of water that the crop can beneficially use.

Irrigated agriculture constitutes a significant portion of total agricultural productivity and profit. Fereres and Connor [3] pointed out that only 17% of agricultural land is irrigated across the globe; however, it accounts for approximately 40% of the total agricultural products. In the United States, only 5%–7% of the total agricultural land is regularly irrigated [4], and yet, it is responsible for over 50% of total crop income [5]. Though only a fraction of the total agricultural land area, the water use for irrigation accounts for over 60% of the total fresh water withdrawals world-wide [2]. In the United States alone, 484.5 billion liters of water per day are used for irrigation [6]. Therefore, irrigation efficiency is extremely important, particularly in water-scarce regions of the world. Over irrigation can not only waste valuable water, but also harm soil productivity by leaving residual chemicals or toxins in the soil when the excess water evaporates [7]. On the other hand, under irrigation can lead to sub-optimal crop yields [8]. Therefore, for advanced irrigation efficiency and beneficial water use, optimal irrigation scheduling is required. Traditionally, irrigation scheduling is accomplished by measuring plant-water stress or soil moisture deficits [9]. Knowledge of the soil moisture profile during the irrigation cycle is essential to achieve maximum irrigation efficiency. Soil moisture at shallow depths is known to be extremely variable temporally [10] and can show significant variability with depth (z) [11]. Therefore, frequent *in situ* soil moisture monitoring is required. In technologically-advanced operations, the irrigation equipment can be linked to soil moisture probes in the field that can regulate the amount of water applied. However, it is often the case that rules of thumb are followed based on known or assumed evaporation rates for the area. At best, these rules are crude, since they are not based on real-time information (weather, soil moisture states, *etc.*) and often lead to poor irrigation efficiencies. Therefore, there is a need for a low-cost method to accurately monitor soil moisture during the irrigation cycle.

During the irrigation cycle, the available information includes the application rate and the total applied water at any time. The distribution of this water within the root zone will not be known unless multi-layer soil moisture probes are employed. Yet, this distribution can be of vital importance to the crop sustainability due to the distribution of plant roots within the zone. The uptake of water by the plants is a function of root mass and suction pressure, both of which vary vertically within the soil profile. Thus, an accurate estimate of the vertical soil moisture distribution is critical to control irrigation rates in real time.

There have been multiple studies in the past addressing the development of a vertical soil moisture profile from limited available information. Broadly, the approaches can be categorized as: regression [12–14]; inversion [15]; knowledge based [16,17]; the water balance approach [18,19]; probabilistic [20–22]; and intelligence [23,24]. Most of the recent studies are hybrid in nature and focused more on total soil moisture estimation rather than soil moisture as a function of depth [22].

Data assimilation techniques can be utilized to improve the soil moisture state in both hydrological and atmospheric models [25]. There have been many previous studies where soil moisture states have been treated as random variables in one way or another [21,22,26–29]. Pachepsky *et al.* [21] provided a comprehensive review of how information theory could be applied to soil moisture transition states. Following this theory and building on recent work in the field, the objective of this study was to develop an entropy-based model that will allow for easy and cost-effective monitoring of irrigated soil moisture states.

2. Soil Moisture States and Irrigation

Irrigation is employed to enhance crop yields in many places in the world, even those that have sufficient rainfall on an annual basis. In many cases, the precipitation is not distributed uniformly throughout the year, so that growing season rainfall may not be sufficient to supply crop requirements on a sustainable basis [30]. The method chosen for the delivery of irrigation water is an important element in determining irrigation efficiency. Low-cost methods include simply flooding the field, either entirely (border irrigation) or by rows (furrow), while more technologically-advanced methods include spraying (pivot or linear systems) or via perforated lines buried in the root zone (drip).

Surface irrigation methods rely on a complex infiltration process that is related not only to soil properties, but also to processes by which the plants uptake water from the soil. The soil moisture infiltration/transpiration process is complex, and a number of models have been proposed to simulate it [31]. Infiltration of water into a porous media proceeds in three stages [32]: on first contact, the soil particles absorb water depending on the organic content of the soil; next, water will begin to wet the surface of the particles; and finally, the water will begin to fill the pore spaces between the particles until the soil matrix becomes saturated (pore spaces are filled to capacity). Water will tend to move in the soil from a wetter area to a drier one through a combination of diffusion and advection processes. Under these forces, water will drain vertically from the soil until it reaches field capacity, which is the water volume held in the pores against gravitational forces. However, plant root uptake can continue until the wilting point is reached, *i.e.*, the point at which negative pore pressures in the soil counteract the root uptake forces. At this point, movement of moisture within the soil column is theoretically ended.

The one-dimensional (vertical) infiltration process is described by the Richards Equation [22]:

$$\frac{\partial \theta}{\partial t} - \frac{\partial}{\partial z}\left(K\left(\theta\right)\frac{\partial \psi}{\partial z}\right) + \frac{\partial K\left(\theta\right)}{\partial z} = 0 \tag{1}$$

where θ = soil moisture content, K(θ)= hydraulic conductivity at θ (mm/h) and ψ = suction head (mm). There is no analytical solution of Equation (1) for general initial and boundary conditions, but a number of commonly-employed analytical infiltration models are designed to simulate it to some degree [31]. There are many uncertainties associated with any method, with estimated soil properties being the source of perhaps the largest uncertainty in the process. Properties estimated in laboratory settings rarely equate to actual field values; thus, characteristic tables usually give a mean (or median) value for a particular soil with a large spread around that value, sometimes encompassing orders of magnitude [31]. In addition, there is no a clear relationship between soil properties and actual behavior (θ *vs.* k(θ) for example), and many different models have been proposed to explain these relationships [33]. There have been multiple

infiltration models commonly used in hydrology, agricultural applications and watershed management, such as [34–37], *etc*. The uptake of moisture by plant roots depends on many plant characteristics (root distribution, for example), which are difficult to predict.

It is well known that soil moisture movement and its associated distributive processes are inherently complex. These complexities pose significant limitations on the ability to physically model the system. Several authors have argued that soil moisture's uncertainties and complexities can be best described through the description of its entropy [21,27,28,38].

3. Entropy Applied to Soil Moisture States

In the classic Shannon entropy formulation, the information associated with a system in state i, is given as [39]:

$$I_i = ln\left(\frac{1}{p_i}\right) \tag{2}$$

where p_i is the probability that the system is in state *i*, and *ln* is the Napierian logarithm.

Then, on average, the information content of the data related to the state is given by the Shannon entropy Function, which is just the negative expected value of the log probability:

$$H = -\sum_{i=1}^{n} p_i ln\left(p_i\right) \tag{3}$$

or, in the continuous case: $H=\int_0^\infty f\left(x\right) ln\left(f\left(x\right)\right) dx$:, where *f(x)* is the continuous pdf.

As pointed out by Pachepsky *et al.* [21], the fluctuation of entropy as the system transitions between states is given by:

$$\sigma_{i,j}^2 = \sum_{i,j}^{n} p_{i,j}\left(ln\left(\frac{p_i}{p_j}\right)\right)^2 \tag{4}$$

Thus, the information content of the data associated with the system can be defined by a probability distribution. According to Mays *et al.* [27], the information entropy is a measure of the correspondence between a probability distribution function (pdf) constructed from a dataset associated with a system and the pdf associated with minimum information about the system. For a situation where minimum information is known *a priori* or the system is unpredictable, the pdf will be uniform, and the entropy will be high [21,27]. Incidentally, in the case of maximum entropy, $\sigma_{i,j}^2$ will be zero [21].

The maximum entropy formulation was developed by [40,41]. The principle of maximum entropy (POME) proposes that if inferences are to be made based on incomplete information, they should be drawn from the probability distribution that has maximum entropy permitted by the information that is already available [42]. Based on this concept, Al-Hamdan and Cruise [22] developed an entropy-based model for simulating soil moisture profiles corresponding to all phases of the physical process. The model was then incorporated into a more general hydrologic formulation given by Singh [28] and further evaluated by Singh [43].

4. Soil Moisture Profile Development Models

4.1. Development of Soil Moisture Profiles from POME

Al-Hamdan and Cruise [22] developed a set of soil moisture profiles assuming a uniform distribution throughout the soil column. The method was based on an approach originally employed by Chiu [44] to compute vertical velocity distributions in open channels. Development of three distinct soil moisture profile possibilities exist: first, as water is applied to an initially dry soil, the column will be wetter near the surface and decrease thereafter, as shown in Figure 1 below (solid line). Then, after a wetting event, the profile will be dry in the upper layers, but retain moisture in the bottom of the column, thus exhibiting one of the profiles shown in the dashed or short dotted lines in Figure 1, depending on the time since the wetting. The case of the parabolic shape (dashed line) is referred to as the dynamic case [22] and may develop in the hours immediately after the event.

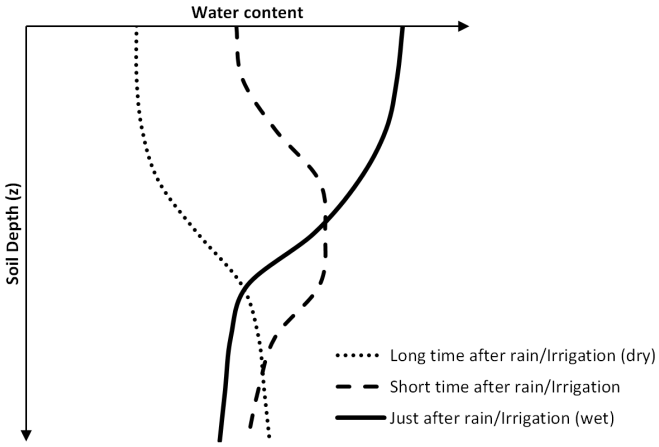

Figure 1. Possible soil moisture profiles

The application of POME to develop a one-dimensional soil moisture profile requires two constraints: the total probability constraint:

$$\int_{\Theta_L}^{\Theta_0} f(\Theta)\, d\Theta = 1 \tag{5}$$

and the constraint to satisfy mass balance:

$$\int_{\Theta_L}^{\Theta_0} \Theta f(\Theta)\, d\Theta = \overline{\Theta} \tag{6}$$

where Θ is the effective saturation and computed as $\frac{\theta-\theta_r}{\eta-\theta_r}$, whereas $\overline{\Theta}$ is the mean value of the soil column, η is soil porosity and θ_r is the residual water content of the soil; Θ_0 and Θ_L are the surface and bottom effective saturations. The second constraint serves to connect the first moment in probability space to the mean water content of the soil column in physical space. The Shannon [39] entropy is given by:

$$I = -\int_0^{\infty} f(x)\, ln\,(f(x))\, dx \tag{7}$$

where *f(x)* is the probability density function of the variable. Maximizing I in Equation (7) for the uniform pdf subject to the constraints above, Chiu [44] developed the 1D profile of a variable decreasing

monotonically from the surface down (wet case) using the method of Lagrange multipliers (put into soil moisture terms by Al-Hamdan and Cruise [22]:

$$\Theta(z) = \frac{ln\left[exp\left(\lambda_2\Theta_0\right) - \lambda_2 exp\left(1-\lambda_1\right)\left(\frac{z}{L}\right)\right]}{\lambda_2} \tag{8}$$

The Lagrange multipliers ($\lambda's$) can be solved from application of the constraints and boundary conditions: surface effective saturation, Θ_0, effective saturation at the bottom of the column, and mean effective saturation value of the soil column ($\overline{\Theta}$); z is the calculation depth, and L is total depth of the column.

Following the same procedure, Al-Hamdan and Cruise [22] developed the profile for the second case (monotonically increasing vertically, *i.e.*, dry case):

$$\Theta(z) = \frac{ln\left[exp\left(\lambda_2\Theta_0\right) + \lambda_2 exp\left(1-\lambda_1\right)\left(\frac{z}{L}\right)\right]}{\lambda_2} \tag{9}$$

Relationships between the Lagrange multipliers and the constraints and boundary conditions have also been developed, as in the first case, with the resulting system of nonlinear equations solved for the multipliers by a technique given by Barbe *et al.* [42]. Finally, Al-Hamdan and Cruise [22] demonstrated that the third case (dynamic) can be handled by a combination of the wet and dry profiles.

4.2. Physically-Based Soil Moisture Model

In order to further evaluate the entropy procedure against profiles that are possible, but may not be present at the validation side, a mathematical model simulating the physics of infiltration, drainage and plant uptake was constructed for the test field. To simulate soil moisture processes in the root zone, a one-dimensional model accounting for the root distribution throughout the root zone [45], as well as the soil water drainage and availability [46] was developed. The total vegetative water extraction is determined using a semi-empirical root water extraction term S that can be expressed as a function of S_{max}, *i.e.*, maximum potential transpiration and a soil water availability factor (α):

$$S(t) = \alpha S_{max}(t); \quad \alpha \leq 1 \tag{10}$$

The soil water availability factor accounts for a restriction of transpiration in either a soil moisture deficit in which the suction capacity of the soil exceeds that of the root or in an excess of soil moisture where the plants are unable to uptake water due to insufficient aeration [47]

To simulate drainage, water is allowed to move vertically in each soil layer modeled if the water content is above field capacity and the layer below is below saturation. The amount of water that moves from one layer to the next is calculated on the storage routing methodology of the Soil Water and Assessment Tool (SWAT, [46]). A full description of the physically-based mathematical model used in this study is provided in the Appendix.

The model offers a significant opportunity to evaluate the ability of the POME-based procedure to simulate the temporal evaluation of the soil moisture profiles in a realistic manner. The model simulates all aspects of the movement of moisture in the soil column, including drainage, soil evaporation and plant transpiration (T_p). It can be used in a combination of wetting and drying episodes to generate profiles

that are realistic for the test soils, but may not be evident in the actual data at the validation site. Thus, a more robust evaluation of the POME method to simulate these complex cases is possible.

4.3. Temporal Evolution of Soil Moisture Profiles by POME

One of the key needs in the development of POME-based moisture profiles is the ability to simulate the temporal movements of moisture in the soil column in conjunction with the application of POME. This issue has not been settled in the past, with previous authors merely advancing the profile one soil layer for each time step without regard to the actual physics involved. By employing a simple mass balance algorithm, this issue can be effectively solved and, thus, allows for the efficient computation of the evolution of soil moisture profiles by POME at virtually any temporal resolution. It was found that through the process of closing the mass balance at each time step, the depth within the soil column to which the moisture has reached is inevitably revealed. Given the soil porosity, only a certain amount of moisture can be contained in a soil column of a given depth. Since, in irrigation simulations, the amount of water applied at each time step is known, it is a simple matter to determine the depth required to meet the mass balance constraint in the POME model at each time step. The procedure consists of two steps. First, the mass of water within the POME-generated profile is checked against the known mass in the soil column. If the mass check does not agree to within 1%, then the moisture in the bottom layer is adjusted, and the POME profile is re-calculated with the new lower boundary condition. If the mass balance in the profile agrees with the known mass, then this indicates that more water can be applied, and thus, the time step is incremented. Second, after mass balance is achieved, the moisture content of the lowest current layer in the profile is checked against its initial value. If the initial value is less than the current value, then the profile depth is maintained. On the other hand, if the current value is greater than the initial, this indicates drainage into the next layer, and thus, a layer is added to the profile. These checks are performed at each time step. Thus, for the first time, the physics of the process are explicitly entered into the POME computations. Since sufficient data are not available at the validation site to fully test the procedure, the physically-based model described previously can be utilized for that purpose.

5. Study Area

The study area is an irrigated corn (maize) field located in Toney (Madison County), Alabama (latitude $34°; 54'$, longitude $86°; 36'$). The field is under center pivot irrigation. Alabama is a subtropical, humid region in the Southeastern United States and receives over 1400 mm of precipitation annually [30]. However, less than 300 mm of precipitation occurs during the growing season, on average, and thus, water-intensive crops, such as corn, can benefit greatly from supplemental irrigation [48].

The field covers 30.5 ha (75.5 ac) comprised of six different soil types. The soil properties as weighted averages in depths of 100 cm are shown in Table 1. The study area was selected due to the fact that a U.S. Department of Agriculture Soil Climate Analysis Network (SCAN) monitoring station (2078) is located adjacent to the field. This site provided hourly soil moisture and climate observations used in the verification of the methodology. Soil moisture is measured with a dielectric probe, and climate data include precipitation, temperature, relative humidity and wind speed and direction.

Table 1. Soil characteristics at the Soil Climate Analysis Network (SCAN) site, as well as the study field.

Soil Type	Sand%	Clay%	θ_{wp} (cm^3/cm^3)	θ_{fc} (cm^3/cm^3)	θ_{sat} (cm^3/cm^3)	K_{sat} (mm/h)	Bulk Density (gm/cm^3)
Ad (SIL)	08.5	33.3	0.204	0.379	0.512	6.30	1.29
Co (SIL)	17.9	35.1	0.216	0.372	0.498	5.11	1.33
Dt (SIL)	18.4	26.7	0.174	0.347	0.490	8.11	1.35
Gs (SIL)	40.8	20.6	0.137	0.288	0.459	15.49	1.43
Df (SICL)	09.5	53.3	0.310	0.432	0.534	2.52	1.24
Dc (SIC)	18.4	47.6	0.286	0.414	0.507	1.92	1.31
SCAN	08.7	48.8	0.287	0.426	0.508	1.41	1.30

6. Methodology

The study consisted of the following elements:

- Verification of the entropy soil moisture profiles with all known input parameters for all cases shown in Figure 1 using observed data from the USDA SCAN site located beside the field.
- Verification of the entropy soil moisture profiles with derived input parameters at the SCAN site.
- Application of the entropy method to simulate a complete irrigation cycle of the center pivot on the field and comparison with a physical model.

The initial task of the entropy validation takes a two-step approach. Initially, errors within the POME model are quantified against observed data with all known input parameters. This is equivalent to the laboratory experiments given by Al-Hamdan and Cruise [22] and Singh [28] and can be compared to those results. Then, further validations of the model results are done using parameters derived only from weather records. The second stage of validation includes the incorporation of the ET and drainage algorithms to adjust the total mass of water in the soil column. This simulates the information that would be available to the user in near real time. This type of field validation of the method has never been done before. The model performance was evaluated using mean absolute error (MAE), as well as Nash–Sutcliffe (R^2_{NS}) efficiency statistics [49]. The R^2_{NS} is recommended for hydrologic error analysis by the American Society of Civil Engineers (ASCE) [50].

$$MAE = \frac{1}{n}\sum_{1}^{n}|(x_{obs} - x_m)| \tag{11}$$

$$R^2_{NS} = 1 - \frac{\sum_1^n (x_{obs_i} - x_{m_i})^2}{\sum_1^n (x_{obs_i} - \overline{x}_{obs})^2} \tag{12}$$

Here, x_{obs} and x_m are the observed and modeled values. The R^2_{NS} values ranges from $-\infty$ to 1, where 1 represents a perfect fit between model and observed values. Any negative result indicates that the mean would have been the better representation for the observed data, whereas a positive result indicates some model skill. The more positive the value, the more accurate the model predictions.

Once the POME model was validated, it was applied to evaluate the continual soil moisture states throughout a specific irrigation strategy (center pivot in this study). Center pivots operate by rotating a boom about a hub located near the center of the field (Figure 2 background). Water enters the boom through the hub, and flow rates and pressures can be regulated via a computerized control system. Most fields will contain multiple soil types (as shown for our test field in Figure 2), and the boom must stay in place until the soil with the maximum water deficit is irrigated to the desired degree.

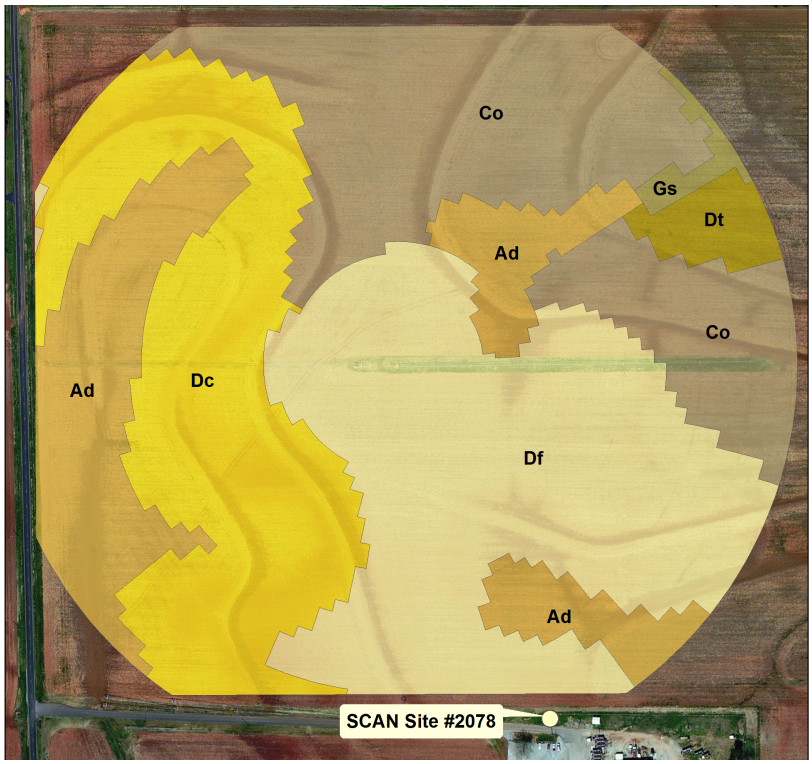

Figure 2. Study area and SCAN site (2078) location.

The level at which the soil should be irrigated is the vital question to be answered. On the one hand, irrigation should not be applied in excess of field capacity lest the water drain out of the soil column and be lost, while on the other hand, sufficient water should be applied to supply plant requirements. The plants use water not only in the photosynthetic process, but they also sequester water in their biomass. Traditionally, irrigation strategies depend on estimated water loss due to climatological estimations of ET or simply examining the surface soil moisture by hand. The optimum irrigation strategy would be to bring the root zone to its field capacity without exceeding it.

One way to accomplish this would be to slightly exceed field capacity in the preceding layers of the soil profile while approaching moisture levels slightly below field capacity in the subsequent layers. This allows the excess water in the preceding layers to drain into the subsequent layers, thus raising their water content to near field capacity, while minimizing the possibility that water will drain out of the soil altogether. This does, however, increase the potential that the plant could become stressed briefly in the upper layers due to over saturation before drainage becomes effective. Evaluation of this strategy would be impractical using soil moisture probes. A physical model would need to be calibrated for each soil type and horizon encountered. However, computation of the complete vertical soil moisture profiles by POME offers an ideal guide for monitoring the moisture in each soil layer.

6.1. Irrigation Phase Simulation

The main purpose of this study is to assess the applicability of the entropy approach to evaluate soil moisture profiles during an irrigation cycle (start of irrigation through the drying phase). The POME model was run to simulate soil moisture states during an irrigation event as the sprinkler boom cycled across the field. The active irrigation phase is represented by the POME wetting front (Equation (8)), whereas the succeeding drying phase (through ET) is represented by the dynamic case runs (Equations (8) and (9) applied successively). Initial surface moisture content for each soil was assumed at 50% of the available water capacity (field capacity minus wilting point). Further, the vertical soil column was assumed to be approximately uniform with each layer at similar soil moisture contents initially. The initial surface values are presented in Table 4 in Section 7.2.

During irrigation, the sprinkler boom crossed multiple soils at each position, as shown in Figure 2. Therefore, the spraying rate was made variable and was kept consistent with the infiltration capacity of each soil type encountered to limit any possible water loss as surface runoff. Infiltration capacity was calculated using the Green–Ampt [34] infiltration equation. The wet case POME model was applied initially at the top layer (15 cm) assuming the surface at saturation and the moisture content based on the initial profile. The mean effective moisture content was calculated as: $\overline{\Theta} = (W_D - W_1)/(T_{depth} - L_{depth})$, where W_D and W_1 are the mass of water content (in units of length) in current soil column depth (D) and the surface, respectively; T_{depth} and L_{depth} are total and layer depths. The procedure described in Section 4.3 was then followed to allow the profiles to evolve with time. The process was repeated, adding each layer successively, until the moisture content at 100 cm demonstrated an increment. This continued until each soil in the boom's path was irrigated. As each soil reached its optimum irrigation level, the spray was cut off in that section of the boom, but continued for soils that had not yet been fully irrigated. When all soils reached their optimum irrigation level, irrigation ceased at the particular position, and the sprinkler boom moved to the next position. A simplified wetting front development process using the POME model is shown in Figure 3.

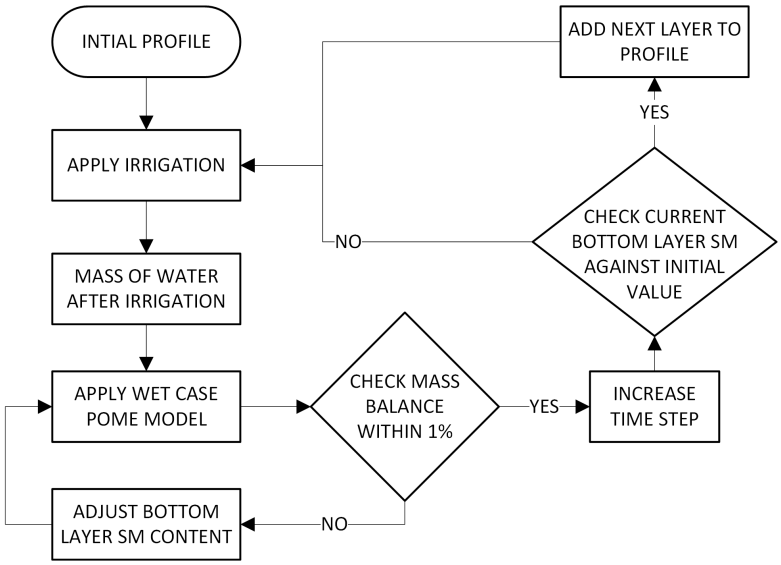

Figure 3. Schematic of the wetting front development using the principle of maximum entropy (POME) model.

6.2. Drying Phase Simulation

As soon as irrigation ceases, the boom changes position, and the drying phase begins. Since the processes associated with this phase (ET and drainage) occur more slowly, the time step is changed to daily, particularly since there is no effective means of computing hourly ET estimates. As shown in Figure 1, immediately after a rainfall/irrigation event, soil moisture profiles usually are not monotonic and tend to develop an inflection point (dotted line in Figure 1). As mentioned previously, the POME model requires three inputs: the upper and lower boundary conditions (surface and bottom layer effective soil moisture contents) and the total water in the soil column for calculation of the mean constraint. As in the wetting case, mass balance was allowed to determine the lower boundary value. This also allowed the calculation of the volume of water that would reach the boundary and, thus, possibly be lost to the system (non-beneficial use of water). The surface moisture value is adjusted daily via a drainage calculation based on an exponential decaying function suggested by Neitsch *et al.* [46], where the decay factor is a function of the average water content of the particular layer. Plant transpiration and soil evaporation were calculated to decrease the daily total mass of water in the soil column. The standard United Nations Food and Agricultural Organization Drainage Paper 56 [2] method, which employs a standardized version of the Penman–Monteith approach, was used and adjusted to correct for actual ET due to limiting of soil moisture. The correction was via an exponential function proposed by Poulovassilis *et al.* [51], where the decay rate is a function of average moisture content and potential evapotranspiration . Wu *et al.* [52] showed that for mature corn crops, nearly 90% of the roots are distributed within top 60-cm depth. For simplification, the ET is uniformly distributed among the top 60 cm of the soil column.

In past work, no method of determining the inflection point on the dynamic profile has been presented. Therefore, a method was needed to be developed for this exercise. In order to find the inflection point on the POME moisture profiles, an approach based on the redistribution of water above field capacity was adopted. It was reasoned that the inflection point would most likely initially occur at field capacity, since vertical drainage would cease at that point, although ET would still be withdrawn during subsequent time periods. Figure 4 demonstrates this point at the USDA SCAN site, where soil moisture profiles are shown based on several different amounts of applied water. In each case, moisture must be redistributed between the upper and lower soil layers until the inflection point (e.g., field capacity) is achieved. The dots on the curves mark the estimated inflection points with the caveat that in some cases, a single inflection point was not obvious, so a range is indicated. The method was tested against observed data and the results given later in this presentation.

The same methodology as described above was used to derive the inflection points for the field soils. For each soil extant in the test field, the ET and drainage algorithms described above were employed for various amounts of applied water until field capacity was obtained for each soil. Then, in order to simulate the drying phase, the wet model (Equation (8)) was applied initially from the surface to the point of inflection, and then, Equation (9) was applied from the inflection point to the bottom of the root-zone at the daily time step. The overall water content was kept consistent with mass balance, and the process was repeated in a circular fashion throughout the field.

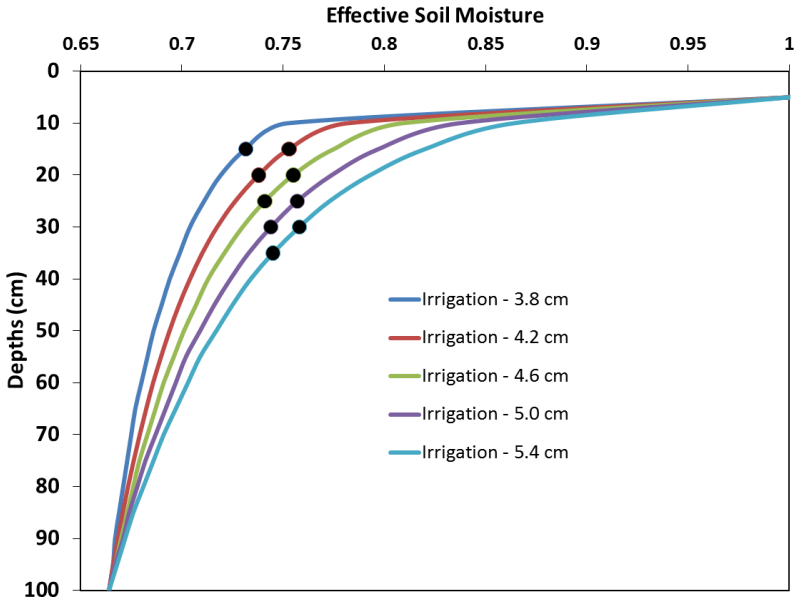

Figure 4. Results of derived inflection points at multiple applied water amounts at the SCAN site using the moisture redistribution technique.

7. Results and Discussions

7.1. Verification of Entropy Profiles

7.1.1. SCAN Site Verification

The first step in the study was to verify the entropy profiles against the SCAN site observations. The SCAN site provides hourly data at depths of approximately 5, 10, 20, 50 and 100 cm. Although Al-Hamdan and Cruise [22] and Singh [28,43] provided extensive verification of entropy-based profiles in a laboratory setting, whereas Mishra *et al.* [30] applied POME-generated profiles for crop yield estimations, no verification has been done up to this time using actual field soil moisture data. The verifications were done for all possible cases.

The first case represents a wetting event beginning at 16:00 h on Julian Day 101 in the year 2013 when 26.4 mm of precipitation fell over a period of 12 h. The simulations continued for 11 h during the day. Typical resultant profiles are shown in Figure 5. The results show that a wetting front developed at a depth of 10 cm in the third hour of the event and remained at that depth thereafter. The entropy simulations were run as the simple wetting case, *i.e.*, Equation (8) with no wetting front development. Even so, the average error in effective soil moisture over the 11 simulations was only 2.21%, indicating that even in this simplified representation, the entropy method gave very accurate results. The R^2_{NS} was computed to be 0.86, indicating that the POME model profile results represent the observed values far better than would have been represented by just assuming one layer value equivalent to the observed mean.

The next SCAN site simulation represents the drying case beginning Julian Day 87 (2012). Daily simulations were run in this case over a nine-day period when no precipitation occurred. Incidentally, the daily time step precludes the development of the dynamic moisture profile discussed above. Typical results are shown in Figure 6 below. Again, the entropy simulations appear to be very accurate, resulting

in an average error over the nine days of only 0.75% in effective soil moisture. The mean R^2_{NS} efficiency value for the dry case simulations was found to be 0.95, again indicating an extremely good representation of the dry case observed values by the POME model. Relatively fewer errors in the dry case simulation can be attributed to the fact that the dry case profiles did not develop any noticeable inflection point during the simulation period and remained monotonic.

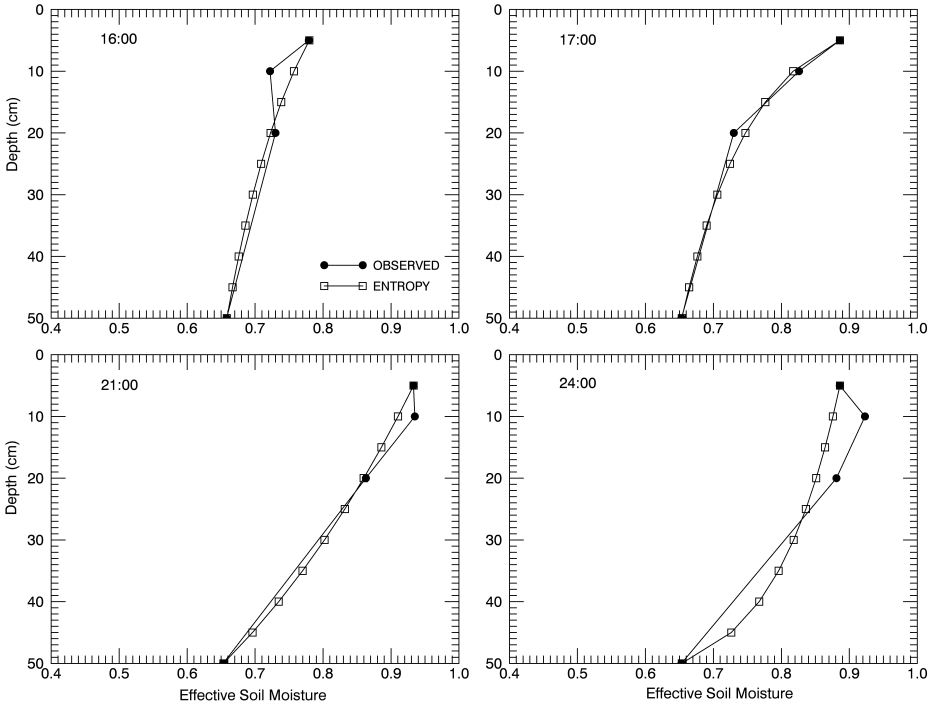

Figure 5. Typical wet case POME-based profiles against SCAN site observed data.

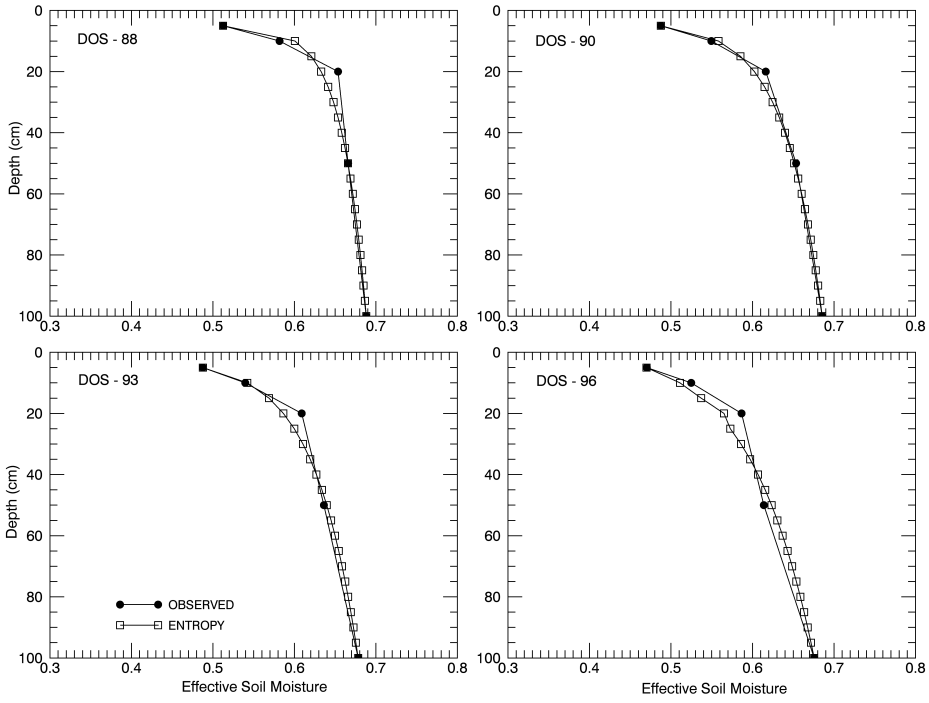

Figure 6. Typical dry case POME-based profiles against SCAN site observed data.

Table 2. Summary of POME-based soil moisture profile results for all possible three cases as compared to the observed values at the SCAN site.

SCAN Site 2078											
	Time/day	**10 cm**			**20 cm**			**50 cm**			R^2_{NS}
		X_{obs}	X_m	e (%)	X_{obs}	X_m	e (%)	X_{obs}	X_m	e (%)	
Wet Case (50-cm Depth)	16:00	0.722	0.757	4.75	0.730	0.722	−1.02	–	–	–	0.56
	17:00	0.826	0.817	−1.14	0.730	0.747	2.32	–	–	–	0.97
	18:00	0.896	0.838	−6.47	0.735	0.768	4.57	–	–	–	0.75
	19:00	0.898	0.842	−6.19	0.764	0.790	3.28	–	–	–	0.81
	20:00	0.896	0.853	−4.74	0.787	0.803	2.08	–	–	–	0.91
	21:00	0.935	0.910	−2.72	0.863	0.859	−0.47	–	–	–	0.98
	22:00	0.935	0.897	−4.08	0.891	0.865	−2.82	–	–	–	0.94
	23:00	0.928	0.886	−4.48	0.886	0.858	−3.13	–	–	–	0.92
	00:00	0.923	0.875	−5.13	0.881	0.851	−3.39	–	–	–	0.89
	01:00	0.923	0.867	−6.02	0.878	0.847	−3.60	–	–	–	0.85
	02:00	0.920	0.861	−6.48	0.876	0.842	−3.87	–	–	–	0.81
Mean *e*				**−3.88**			**−0.55**				**0.86**
MAE (%)				**4.74**			**2.78**				–
Dry Case (100-cm Depth)	88	0.582	0.601	3.26	0.653	0.632	−3.16	0.665	0.665	0.0	0.87
	89	0.562	0.583	3.88	0.636	0.619	−2.67	0.658	0.655	−0.42	0.91
	90	0.549	0.558	1.58	0.616	0.602	−2.26	0.653	0.651	−0.34	0.98
	91	0.549	0.566	3.05	0.621	0.606	−2.33	0.653	0.650	−0.48	0.96
	92	0.547	0.555	1.48	0.616	0.597	−3.11	0.643	0.644	0.16	0.97
	93	0.539	0.542	0.47	0.609	0.586	−3.68	0.636	0.639	0.55	0.97
	94	0.537	0.535	−0.41	0.604	0.582	−3.71	0.634	0.637	0.61	0.97
	95	0.532	0.524	−1.55	0.591	0.570	−3.56	0.626	0.630	0.70	0.98
	96	0.524	0.512	−2.66	0.586	0.565	−3.68	0.614	0.623	1.55	0.96
Mean *e*				**1.01**			**−3.13**			**0.26**	**0.95**
MAE (%)				**2.04**			**3.13**			**0.54**	–
Dynamic Case (100-cm Depth)	29	0.757	0.727	−3.89	–	–	–	0.556	0.574	3.23	–
	30	0.835	0.823	−1.38	–	–	–	0.602	0.629	4.48	–
	31	0.797	0.778	−2.34	–	–	–	0.584	0.620	6.18	–
	32	0.775	0.748	−3.53	–	–	–	0.578	0.611	5.71	–
	33	0.759	0.733	−3.67	–	–	–	0.557	0.595	6.77	–
	34	0.759	0.734	−3.41	–	–	–	0.557	0.591	6.05	–
	35	0.747	0.715	−4.29	–	–	–	0.553	0.587	6.17	–
	36	0.752	0.719	−4.35	–	–	–	0.551	0.574	4.23	–
	37	0.747	0.711	−4.82	–	–	–	0.561	0.581	3.51	–
	38	0.738	0.757	2.63	–	–	–	0.548	0.564	2.83	–
	39	0.738	0.754	2.22	–	–	–	0.548	0.563	2.65	–
	40	0.735	0.750	2.01	–	–	–	0.544	0.559	2.74	–
Mean *e*				**−2.07**						**4.55**	–
MAE (%)				**3.21**						**4.55**	–

The last simulations of the SCAN site were run to verify the dynamic case profiles. Dynamic profiles are characterized by the presence of at least one prominent inflection point. The SCAN site developed such profiles between Julian Days 29 and 40 (2013). The observed data showed that an inflection point was consistently present at 20 cm. In the first simulation, the POME model was applied assuming that this was known, the case corresponding to the laboratory experiments reported by Al-Hamdan and Cruise [22] and Singh [28]. A dry case POME was run initially through 0–20 cm and then a wet case subsequently through the remaining 80 cm (20–100 cm). The dynamic case profiles resulted in a mean absolute error of 2.89% in effective soil moisture as compared to the SCAN site observed values. This compares very favorably to the errors reported earlier by Al-Hamdan and Cruise [22] and Singh [28], which averaged 2.1%. The available R^2_{NS} efficiency statistic was not calculated for this case, since three out of five values available for comparison were provided as input. Typical profiles from the dynamic case are presented in such simulations in Figure 7. A summary table of the entire validation procedure can be found in Table 2.

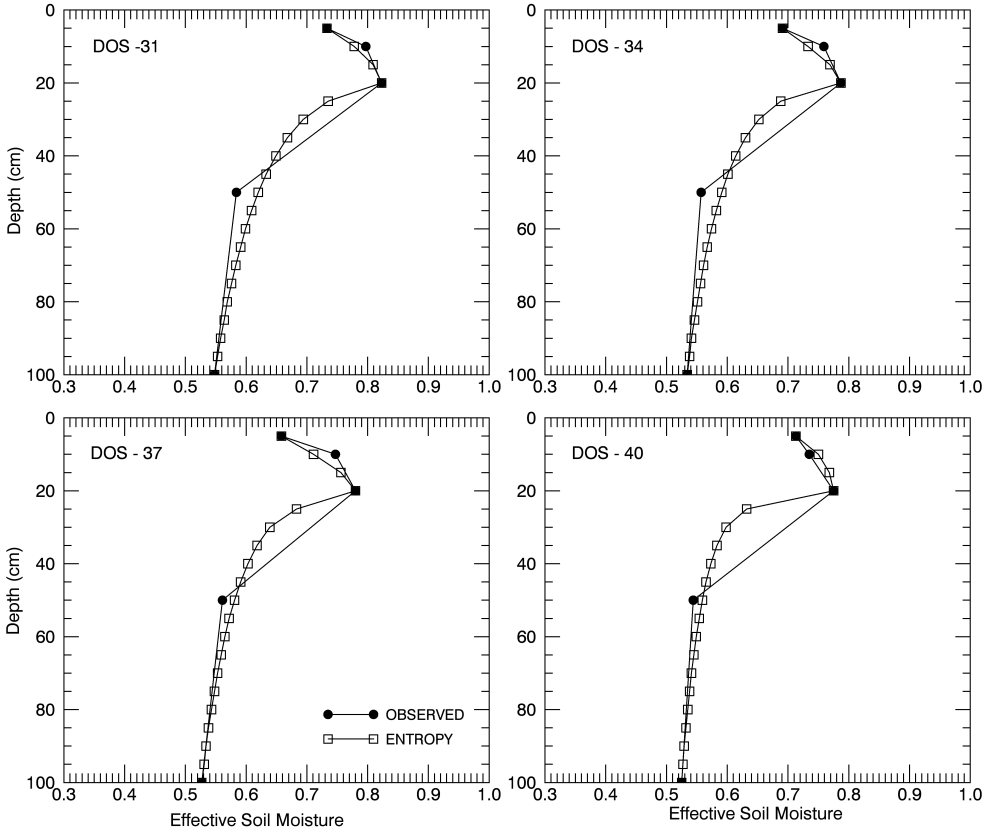

Figure 7. Dynamic case POME-based profiles against SCAN site observed data.

7.1.2. Entropy Validation with Derived Parameters

In the previous validation of the dynamic case, the necessary boundary conditions (surface and bottom effective soil moisture content), as well as the additional input parameters for the dynamic case (the location and moisture content of the inflection point) were assumed known. In a more realistic scenario, the validation was done by estimating these parameters by the methods described above. This simulates

the real-world case where these values would necessarily be unknown to the user. These profiles were then compared with observed SCAN site moisture values to test the robustness of the inputs.

The first step is to select the inflection point on the profiles. Since the assumption is that each soil will have an inflection point located at the point where field capacity first occurs, then the calculations that led to Figure 4 were consulted. The figure shows that for the soil at the SCAN site, the inflection point can vary from 15–35-cm depth depending on the amount of applied water. Therefore, following the premise that the user would have minimum prior information, a mean value of 25 cm was selected as the inflection point depth for these simulations. As discussed, the moisture content at the inflection point was assumed to be field capacity initially. The ET and drainage computations previously discussed were used to compute the surface and mean effective moisture values. While the lower boundary is adjusted if required to keep the mean water content within the upper and lower boundary conditions, the location of the inflection point was kept constant.

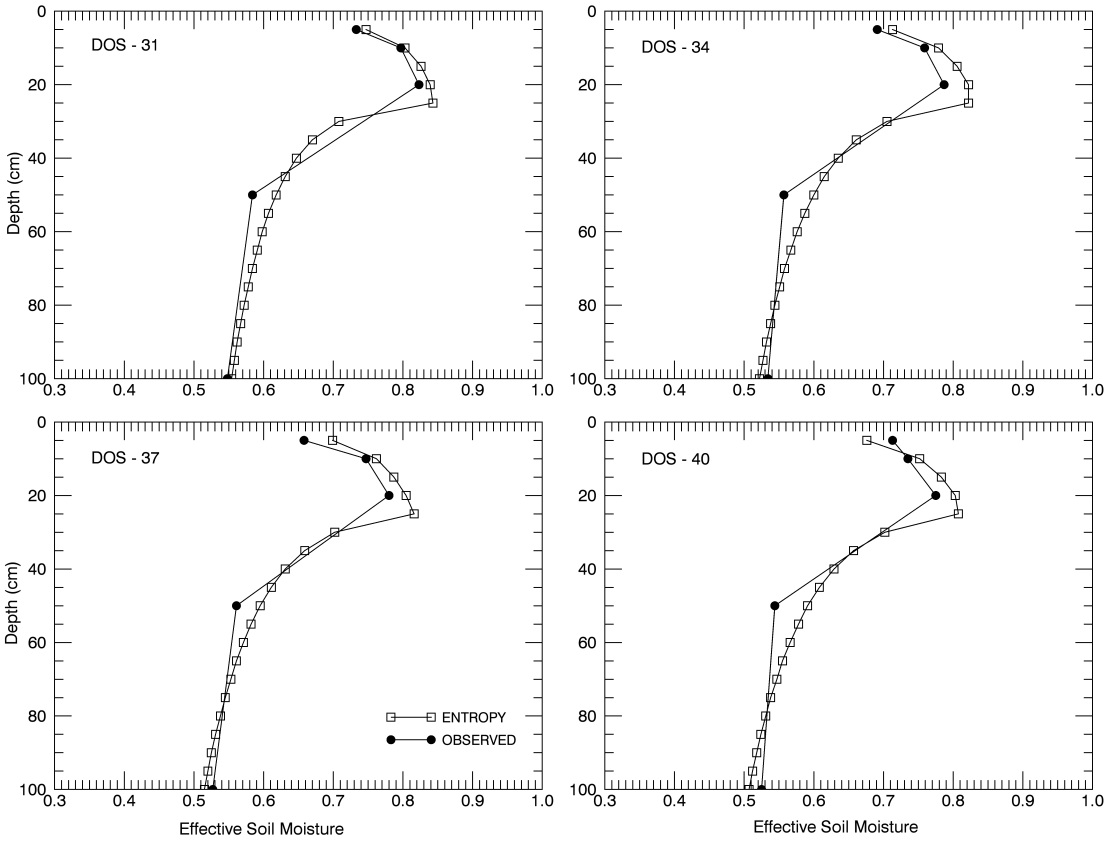

Figure 8. Representative dynamic case POME-based soil moisture profiles with derived inputs parameters against SCAN site observed data.

Typical results of the simulated profiles are shown in Figure 8, and a complete error analysis is given in Table 3. During the 10 days of simulation, the individual layer mean absolute errors ranged from 0.22–8.6% with a mean error of about 3.8%. It can be noted that the actual observed inflection point was 20 cm (compared to the computed of 25), but the difference in inflection point depths still results in acceptable errors across the distribution as a whole. Further, the surface value MAE was observed to be 3.8%, with the highest errors observed at 6.16% and 5.03% on Days 37 and 40, respectively. The higher errors are, in part, due to extremely low ET estimations due to slight precipitation observed on

Days 36 (0.15 cm) and 39 (0.4 cm). Due to this, the surface moisture content observed by moisture probes showed an increase on Days 39 and 40; however, the POME model did not catch this, since it was applied with no additional precipitation/irrigation information. The R^2_{NS} efficiency statistic was computed to be 0.93, verifying that the derived input parameters of the POME model are sufficient in capturing the distribution of the observed soil moisture profile.

Table 3. Summary of POME-based soil moisture profile results for the dynamic case against SCAN site observed data with the derived inflection point, as well as the inflection moisture content.

		SCAN site 2078									
	depth	**DOS**									
	(cm)	**31**	**32**	**33**	**34**	**35**	**36**	**37**	**38**	**39**	**40**
X_{obs}	5	0.733	0.705	0.700	0.691	0.681	0.671	0.658	0.658	0.700	0.713
	10	0.797	0.775	0.759	0.759	0.725	0.752	0.747	0.738	0.738	0.735
	20	0.823	0.804	0.794	0.787	0.783	0.785	0.780	0.783	0.778	0.775
	50	0.584	0.578	0.557	0.557	0.553	0.551	0.561	0.548	0.548	0.544
	100	0.548	0.539	0.537	0.534	0.532	0.530	0.527	0.525	0.521	0.525
X_m	5	0.747	0.725	0.721	0.713	0.707	0.705	0.699	0.687	0.685	0.677
	10	0.803	0.792	0.785	0.779	0.774	0.772	0.762	0.752	0.752	0.752
	20	0.839	0.837	0.829	0.822	0.816	0.813	0.805	0.805	0.803	0.803
	50	0.618	0.608	0.597	0.600	0.594	0.595	0.595	0.591	0.591	0.590
	100	0.554	0.540	0.531	0.522	0.522	0.515	0.515	0.508	0.507	0.507
$e(\%)$	5	1.95	2.98	2.96	3.25	3.90	5.10	6.16	4.34	−2.15	−5.03
	10	0.79	2.18	3.49	2.71	3.68	2.64	2.00	1.95	1.95	2.28
	20	1.98	4.10	4.34	4.45	4.38	3.61	3.12	2.87	3.24	3.56
	50	5.82	5.19	7.13	7.67	7.44	8.05	6.06	7.76	7.76	8.63
	100	1.11	0.22	−1.03	−2.29	−1.87	−2.77	−2.35	−3.26	−2.60	−3.45
Mean *e*	-	**2.33**	**2.93**	**3.38**	**3.16**	**3.51**	**3.32**	**3.00**	**2.73**	**1.63**	**1.20**
MAE (%)	-	**2.33**	**2.93**	**3.79**	**4.07**	**4.25**	**4.43**	**3.94**	**4.04**	**3.54**	**4.59**
$\boldsymbol{R^2_{NS}}$	-	**0.97**	**0.95**	**0.93**	**0.92**	**0.87**	**0.92**	**0.92**	**0.93**	**0.94**	**0.91**

7.2. Application of the POME Model to an Irrigation Cycle

The POME model was used to simulate a complete irrigation cycle for the test field shown in Figure 3. As shown in the figure, at any position, the boom will apply water to multiple soil types. The spray rate was variable across the boom and was set at the infiltration capacity of each soil to avoid producing surface runoff. The boom remained in this position until all of the soils received the optimal amount of water measured as when the moisture profile reached the bottom layer. Not only was surface runoff avoided, but another requirement was to not let excess water drain from the soil to pollute groundwater. Thus, the algorithm was run allowing each vertical layer to become irrigated in turn, until the mass

balance operation required the lower boundary to be increased, thus indicating that water had reached the bottom of the soil. At that point, the irrigation of the particular soil ceases, *i.e.*, the spray stops; however, the boom remains in position until the last soil is irrigated. Table 4 shows the rate of irrigation applied, as well as the total time required for irrigation to reach the 100-cm depth for each soil type. The 30.5 ha field is fully irrigated with 120 radial boom movements. Sprinkler boom movement is governed by the soil with the slowest infiltration rate within the boom range. Out of the total 120 boom movements, 50 times, the Dc soil with the maximum irrigation time (141 min) was covered, and the other 70 times, the second slowest infiltrating soil Df(115 min) was covered. This results in a total of 10.5 days (24 × 7) to irrigate the entire field.

Table 4. Summary of wetting front simulations.

Soil Type	Irrigation Rate (cm/min)	Total time to Saturate (min)	Effective SM		Total Water (cm)
			Surface Initial/Final	Bottom Initial/Final	Initial/Final
Ad (SIL)	0.104	56	0.55/1.0	0.57/.625	29.5/35.3
Co (SIL)	0.104	58	0.57/1.0	0.55/0.632	28.5/34.5
Dt (SIL)	0.102	58	0.52/1.0	0.55/0.584	27.0/32.6
Gs (SIL)	0.101	59	0.44/1.0	0.47/0.513	21.5/27.1
Dc (SIC)	0.019	141	0.65/1.0	0.66/0.665	35.4/38.1
Df (SICL)	0.035	115	0.71/1.0	0.68/0.720	36.3/40.2

The simulation assumes a corn (maize) crop at or near maturity during the growing season in northern Alabama. A total of nearly 14.7 million liters of water was required for a complete simulated irrigation cycle. Figure 9 shows typical soil moisture profile development during irrigation phase simulations.

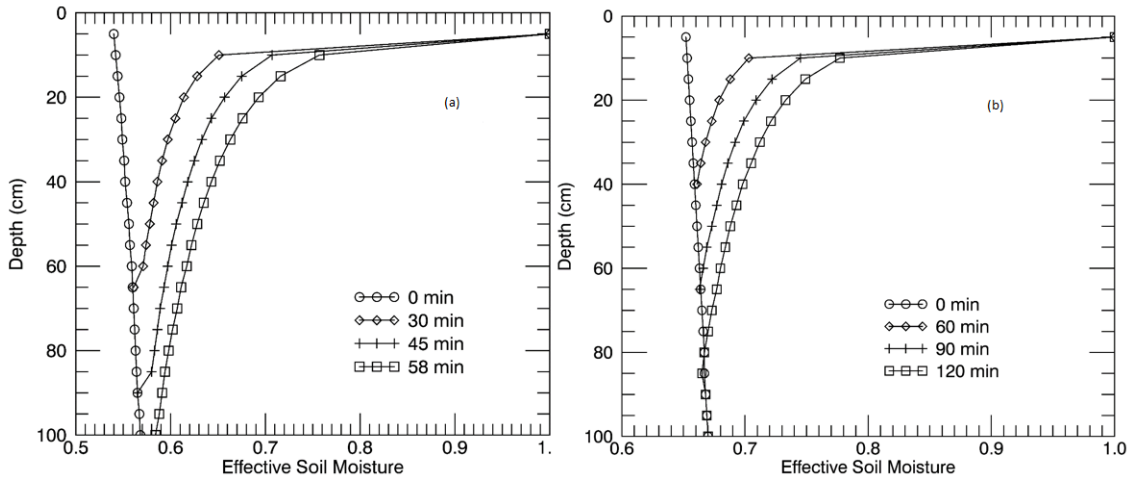

Figure 9. Typical wet case soil moisture profile results during irrigation phase simulation: (**a**) Ad, silt loam soil; (**b**) Dc, silty clay soil.

Once irrigation ceases for a particular area, the drying phase begins at a daily time step. The drying phase is simulated through the dynamic POME model. For soils that develop an inflection point, the

depth and moisture content at that point are additional derived input requirements. By performing the simple mass distribution exercise demonstrated earlier for the SCAN site, inflections points were easily identified. Inflection points were identified for four out the six simulated soil types. The four soils that developed inflection points tended to have higher hydraulic conductivities and lower field capacities than those that did not, further reinforcing the derivation technique.

Table 5. Summary of drying phase simulations: IP is the inflection point depth (cm); A is surface effective SM; B is effective soil moisture content at IP; C is bottom (100 cm) effective soil moisture content; and D is total amount of water (cm) contained in the profile. AET is the actual evapotranspiration in cm of water per day.

		Initial	**200**	**201**	**202**	**203**	**204**	**205**	**206**	**207**	**208**	**209**	**210**
	A	1	0.80	0.72	0.69	0.66	0.65	0.63	0.62	0.59	0.56	0.53	0.50
Ad	B	0.70	0.69	0.67	0.65	0.64	0.63	0.62	0.62	0.64	0.62	0.61	0.60
(IP at	C	0.63	0.63	0.63	0.62	0.62	0.62	0.62	0.62	0.58	0.58	0.58	0.57
20 cm)	D	35.3	34.3	33.8	33.5	33.0	32.8	32.5	32.2	31.7	31.2	30.7	30.3
	AET	–	0.56	0.60	0.53	0.42	0.25	0.27	0.32	0.521	0.48	0.45	0.41
	A	1	0.82	0.74	0.70	0.68	0.66	0.64	0.63	0.60	0.56	0.54	0.51
Co	B	0.72	0.69	0.67	0.66	0.64	0.64	0.63	0.63	0.64	0.63	0.61	0.59
(IP at	C	0.63	0.63	0.63	0.63	0.63	0.63	0.63	0.63	0.59	0.58	0.58	0.57
20 cm)	D	34.3	33.7	33.2	32.9	32.5	32.3	32.0	31.7	30.5	30.1	29.9	29.4
	AET	–	0.56	0.59	0.53	0.42	0.25	0.27	0.31	0.51	0.47	0.44	0.40
	A	1	0.89	0.82	0.77	0.74	0.73	0.71	0.68	0.64	0.61	0.58	0.55
Dc	B	–	–	–	–	–	–	–	–	–	–	–	–
(No	C	0.67	0.67	0.67	0.67	0.64	0.64	0.64	0.64	0.67	0.66	0.66	0.66
IP)	D	38.1	37.2	36.9	36.7	36.3	35.8	35.4	35.2	35.1	34.0	33.7	33.3
	AET	–	0.57	0.61	0.55	0.44	0.27	0.29	0.33	0.55	0.50	0.46	0.42
	A	1	0.89	0.82	0.79	0.76	0.74	0.73	0.69	0.67	0.64	0.61	0.58
Df	B	–	–	–	–	–	–	–	–	–	–	–	–
(No	C	0.72	0.72	0.72	0.72	0.72	0.70	0.70	0.72	0.72	0.72	0.72	0.72
IP)	D	40.2	39.2	39.0	38.7	38.4	37.5	37.3	37.0	36.5	36.1	35.7	35.4
	AET	–	0.55	0.59	0.53	0.42	0.25	0.27	0.31	0.51	0.44	0.41	0.37
	A	1	0.76	0.68	0.65	0.62	0.60	0.58	0.56	0.53	0.50	0.47	0.44
Dt	B	0.65	0.67	0.66	0.64	0.65	0.63	0.63	0.62	0.61	0.59	0.58	0.56
(IP at	C	0.58	0.58	0.58	0.58	0.58	0.58	0.58	0.58	0.56	0.56	0.53	0.53
35 cm)	D	32.6	31.8	31.3	30.8	30.7	30.3	30.0	29.8	29.0	28.5	27.7	27.3
	AET	–	0.59	0.64	0.57	0.46	0.29	0.32	0.37	0.57	0.50	0.47	0.44
	A	1	0.64	0.58	0.54	0.51	0.49	0.47	0.45	0.41	0.37	0.34	0.31
Gs	B	0.59	0.61	0.61	0.59	0.54	0.53	0.52	0.51	0.50	0.48	0.46	0.44
(IP at	C	0.51	0.51	0.51	0.51	0.51	0.51	0.51	0.51	0.51	0.51	0.51	0.51
45 cm)	D	27.1	26.9	26.4	25.9	24.8	24.6	24.1	23.7	23.1	22.5	22.1	21.7
	AET	–	0.59	0.64	0.57	0.46	0.29	0.30	0.35	0.59	0.52	0.49	0.45

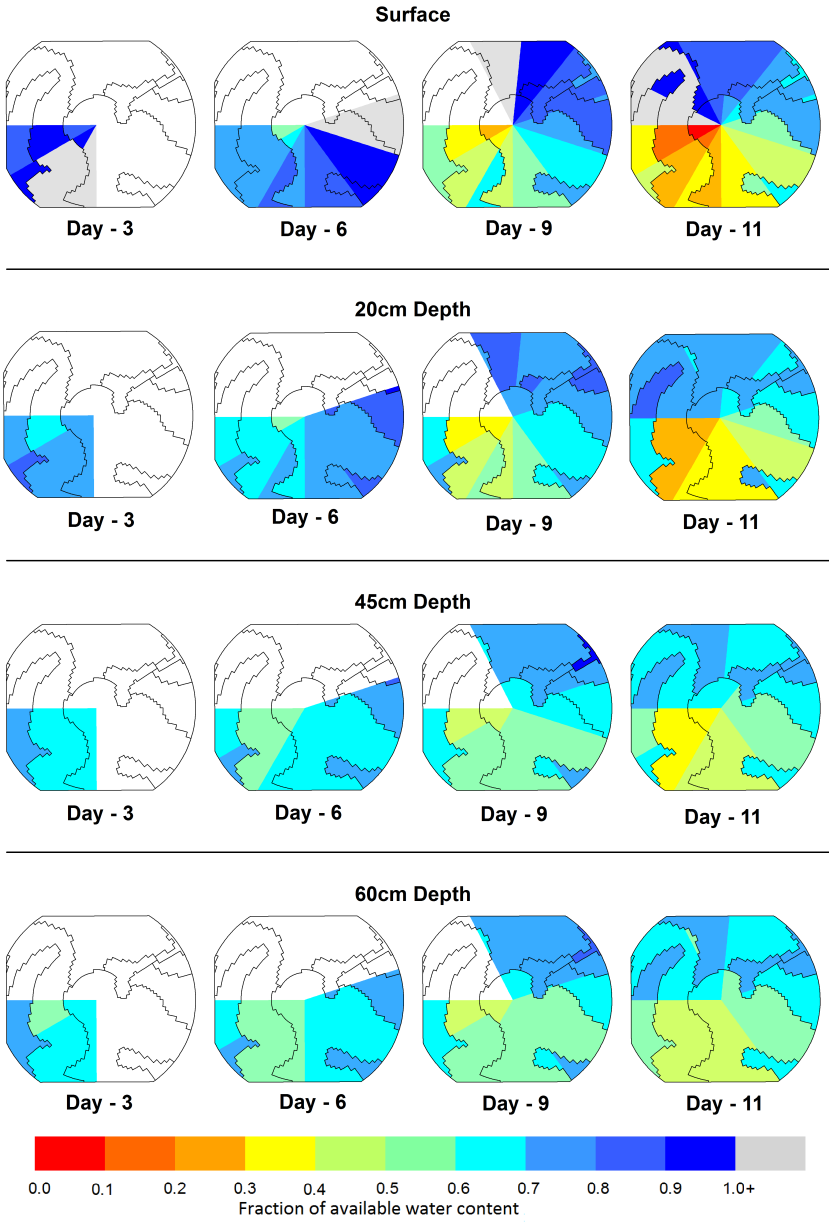

Figure 10. Field map with soil moisture conditions on Days 3, 6, 9 and 12 at the surface; 20-cm, 45-cm and 60-cm depths

The field is divided into 120 radial segments each representing a sprinkler boom spatial extent. Given the 10.5 days required to irrigate the field, then about 11 days of drying will occur for the initially-irrigated segments before the boom would return to its initial position. Thus, the drying phase simulations (dynamic case POME) were run for 11 days. For example, Figure 10 shows the fraction of available water content (θ_{AWC}) for Days 3, 6, 9 and 11 at multiple depths. The portion of the field currently under irrigation usually had a moisture content above field capacity (>100% of AWC) at the surface. As clear from the Figure 10, with the 9 days of drying none of the soils at any depth showed signs of water stress. Soil water stress impact on plants is extremely specific to plant type and it's growth stage [53]. In this study, a rather simple and conservative definition of water stress was used based on Luo *et al.* [54] as moisture content less than 20% of AWC. While only 0.3 ha (0.97% approx.) of the total field showed signs of stress with nine days of irrigation, by the end of 11 days of irrigation, nearly

1.62 ha (5.16%) of the field begain to experience soil moisture stress at the surface. On the other hand the Dc soil with the maximum of 11 days of drying at the surface had the maximum stress of 1.17% of AWC. While only 1.57 ha of the field area had a water content less than 20% of AWC, there is another 3.16 ha of the field fell just outside of water stress limit (20%–30% of AWC) by the end of irrigation cycle. However, at depths 20 cm and below, no soil at any field portion showed a water stress condition. Table 5 shows the summary of the drying phase results at the end of each day. The above results depend on the initial position of the boom itself. If the boom was started from the opposite side of the field, a different portion of the field would be under drying for 11 days.

7.3. Comparison to Physically Based Model

The previous validation of the POME model employed fairly simple observed profiles at the USDA SCAN site. It is known that in some cases, field soils can develop soil moisture profiles that are much more complex than those observed at the SCAN site. In addition, it is desirable to have some basis of comparison of the proposed method on the actual test field. To that end, a complex physically-based mathematical model of soil moisture movement was constructed for the test field. The details of this model are provided in the Appendix. In the model, the mass distribution of water contained in the soil is a function of drainage, ET and its partition, as well as its distribution through the column. Evaporative losses are partitioned between plant transpiration and bare soil evaporation. A root distribution for maize commonly used in crop models was employed in the mathematical model. Inflection points develop naturally as a function of plant root uptake and vertical drainage.

The first goal of any model is to conserve mass. The overall mean error for all soils over the complete drying phase simulation was -1.9%–1.7% ($R^2 > 0.98$ with the physically-based mathematical model). The mass balance closure criteria of 1% and round-off errors can aggregate to slightly increase the total error. However, it appears that the simplified method of estimating inflection point in the entropy model did not unduly bias the method in comparison to the physically-based mathematical model. Figure 11 shows the range of mean mass errors observed by each soil over the 11 days of simulation against the mathematical model.

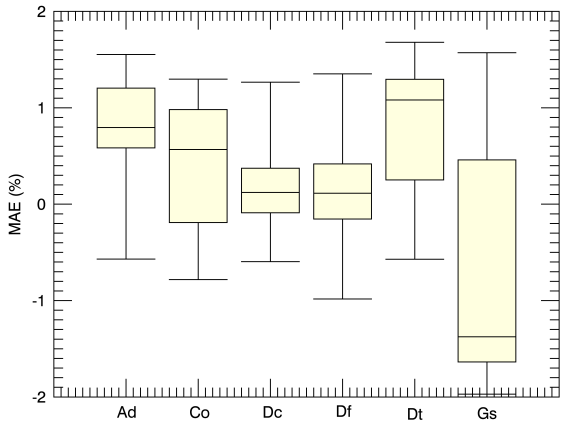

Figure 11. Total mass error of the POME model against the physical based mathematical model.

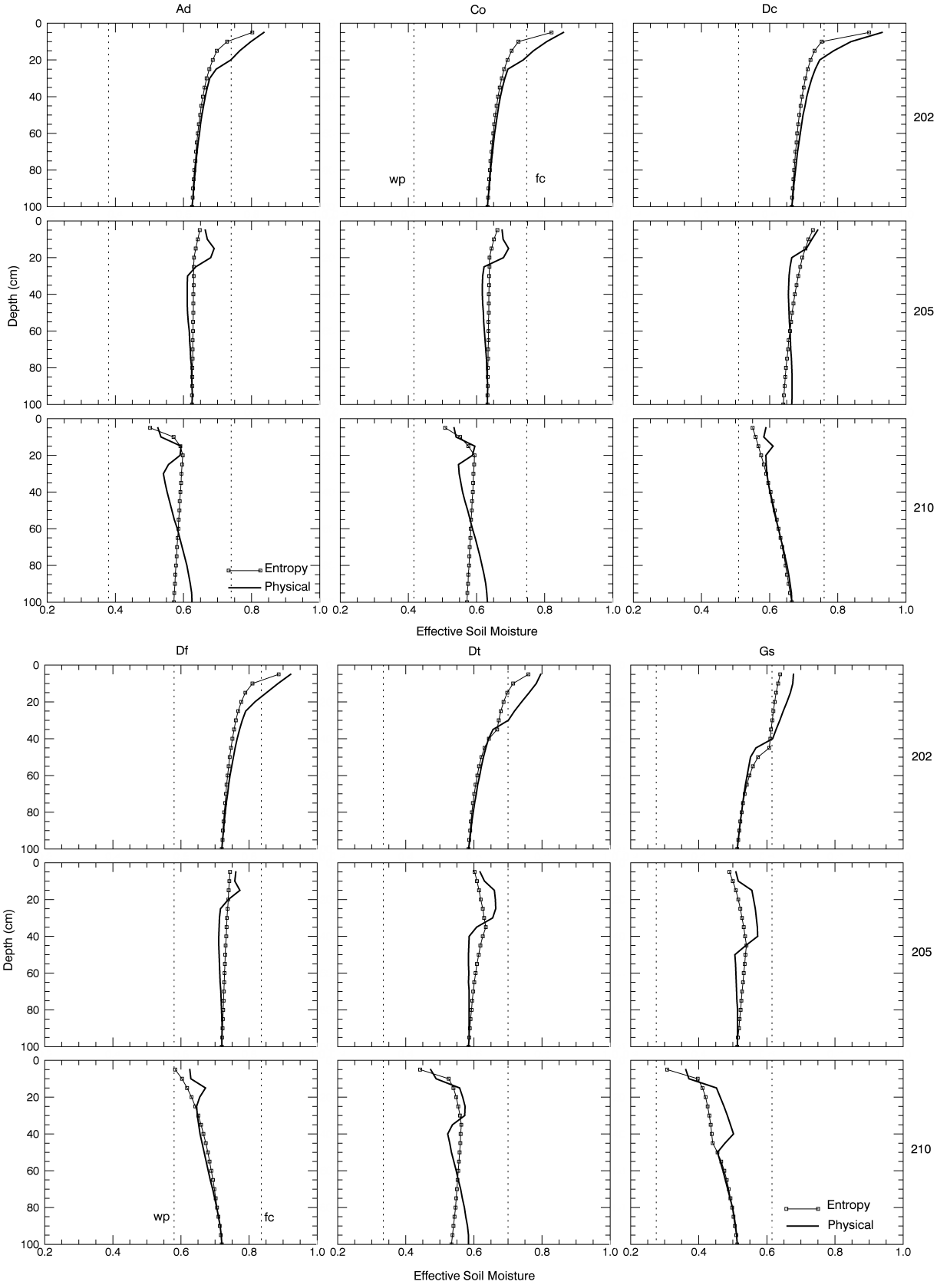

Figure 12. Typical soil moisture profile comparisons between the physical model and entropy generated profiles for Days 1, 5 and 11 of an irrigation cycle. Vertical dashed lines represent the soil-specific effective wilting point (left) and field capacity (right) positions.

After ensuring overall mass balance, the next comparison is by individual soil layers. This would enable quantification of errors associated with derived inflection points, assumption of field capacity at inflection points and distribution of plant transpiration (T_p) and drainage through the soil column. Figure 12 shows some typical profile comparisons of the entropy model *vs.* the mathematical model for each soil type at various stages of an irrigation cycle.

The figure demonstrates how more complex profiles are possible for these soils than were exhibited by the SCAN site data. The combination of the bare soil evaporation routine and the transpiration associated with the root zone distribution resulted in numerous profiles with multiple inflection points that were not observed at the SCAN site and not assumed by the entropy model. Still, the figure shows that, although only one or, in some cases, no inflection points were assumed by the entropy model, the model still came close to resolving the profile in each case, even though it did not know the profile in advance.

An overall error analysis of the profile comparisons is given in the box and whisker plot shown in Figure 13, which summarizes all errors across all layers of the model. Overall, the mean absolute error for all soils together at each layer was about 2.95% (max = 14.87% by Gssoil on Day 11 at the surface). Maximum errors were observed at the surface and around inflection points. Mean error at the surface was found to be 5.8%, whereas errors at the inflection point and 5 cm around it averaged 4.11%. These errors can be mainly attributed to the differences in moisture content due to the development of additional inflection points (see Table 6). Another source of error was associated with the surface and bottom moisture content. The discrepancy at the surface moisture content is again due to the complexity of the physical model, which included crop leaf abstractions/shadow effects on soil evaporation and a complex root distribution, when, of course, these issues were not a part of the entropy model. On the other hand the entropy model's deviation of the bottom moisture content from the mathematical model results from error at the surface and inflection points being carried over to the bottom in order to guarantee the conservation of mass balance over the entire profile.

Table 6. Inflection point development results from the physical model run and the moisture redistribution technique.

Soil Type	Physical model Result		Redistribution Technique Result
	First 2 prominent inflection point depths (cm) (initial)	First 2 prominent inflection point depths (cm) (final)	inflection point depths (cm)
Ad (SIL)	20, 00	15, 25	20
Co (SIL)	25, 00	15, 25	20
Dt (SIL)	30, 00	15, 35	30–40
Gs (SIL)	40, 00	15, 40	45–50
Dc (SIC)	00, 00	15, 00	00
Df (SICL)	00, 00	15, 00	00

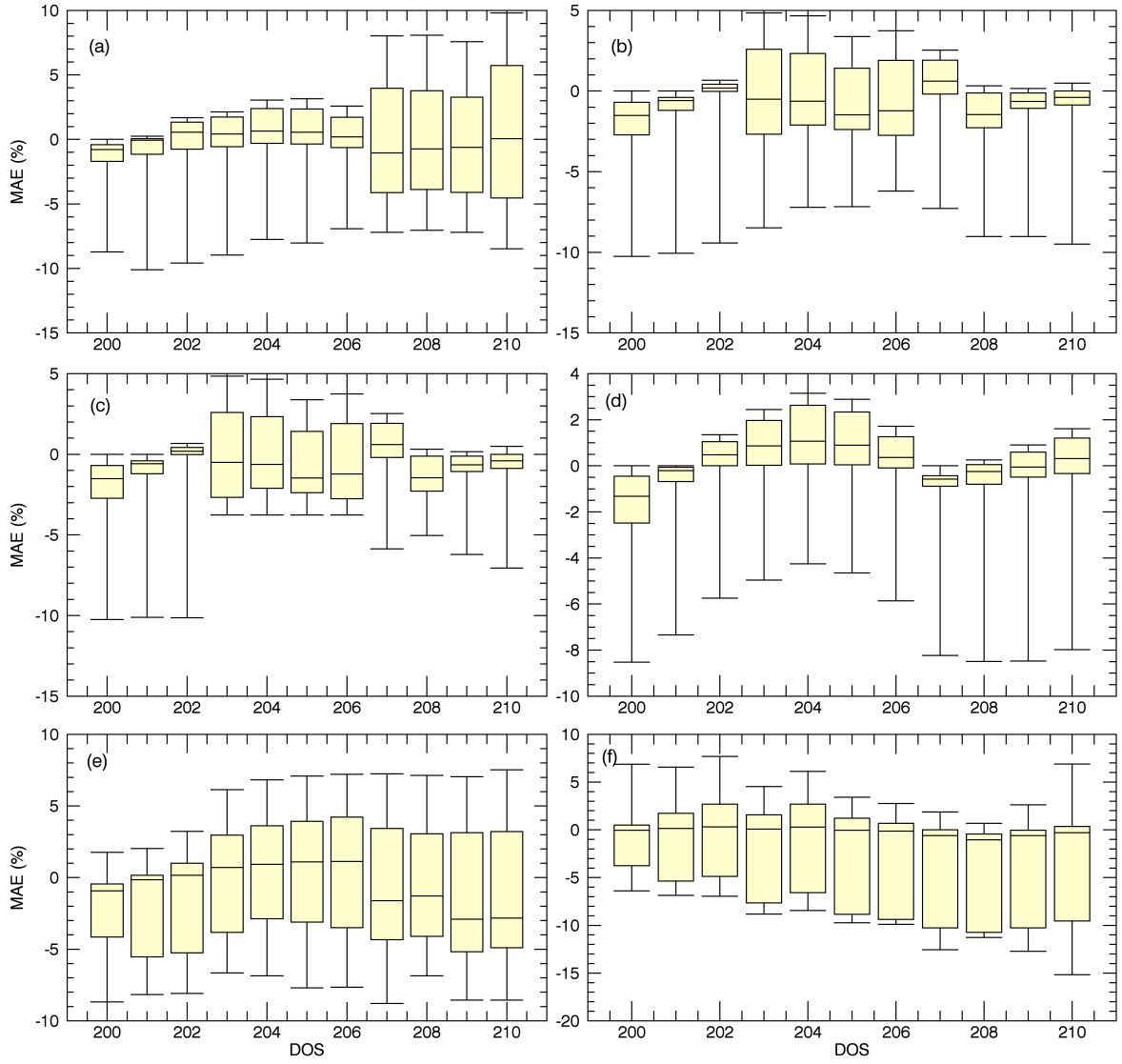

Figure 13. Box plot of errors of the POME model against the mathematical model at layer depths.

8. Conclusions

The purpose of the exercise described here was to validate the POME soil moisture model against observed field data, compare POME to the results of a complex physically-based mathematical model and to demonstrate how POME can be used to monitor and guide an irrigation system with relative accuracy and ease. The comparison of POME to field and model data was discussed above and the errors enumerated. The third purpose of the study is discussed in terms of irrigation efficiency measures and the development of potential plant stress or lack thereof. This discussion revolves around the amount of water added to the field and how that water was used, or wasted, during the irrigation cycle. This information is summarized in Table 7 below.

Table 7. Summary of irrigation efficiency observed by the POME (in cm of water).

Soil Type	Water added	Total ET	ΔS	$\Delta(S+ET)$	ΔSM	ΔSM_{100cm}
Ad (SIL)	5.8	4.81	0.8	5.61	0.19	0.137
Co (SIL)	6.0	4.75	0.9	5.65	0.35	0.198
Dt (SIL)	5.6	5.22	0.3	5.52	0.08	0.081
Gs (SIL)	5.6	5.25	0.2	5.45	0.15	0.096
Dc (SIC)	2.7	4.99	−2.1	2.89	−0.19	0.011
Df (SICL)	3.9	4.65	−0.9	3.75	0.15	0.095

The table shows the amount of water added to each soil class, the actual evapotranspiration for that soil, the change of soil moisture from the initial (beginning of irrigation) state and the volume of water that drained to the bottom of the soil profile. It should be noted that these data relate to the soil moisture column as a whole and not to any particular layer. As discussed in the introductory material, ET demand and enhanced soil moisture states are considered beneficial uses of irrigation water, while surface runoff or vertical drainage to groundwater are not. In this demonstration, the irrigation was applied in a manner to preclude surface runoff, so the principle non-beneficial use of the water would be drainage. In this regard, the table shows that a relatively small percentage of the applied water even reached the bottom of the profile (average of 1.9%). Otherwise, the added water was used to supply ET demands and enhance soil moisture status.

The table demonstrates how the finer texture, silty clay soils (Dc and Df) responded to the irrigation in a fundamentally different manner than did the coarser soils. Since these soils have a smaller water holding capacity, they absorbed considerably less water than the other soils present in the field. However, since the ET demand is set primarily by weather conditions, ET did not vary much over the field, so that the available soil moisture was drawn down in those two cases. The ET and SMdemands were met fairly well in the case of the Df soil, with even a slight overall surplus at the end, while the crops residing on the Dc soil would not fare as well. The overall negative water balance in this case indicates that the soil moisture fell below 50% of the available water capacity (the initial soil moisture condition) considering the column as a whole. In fact, the results indicate that for this particular soil class, the moisture state overall reached about 31% of the available water capacity of the soil. The next question is, would this condition stress the maize plants? Figure 10 can be used to help answer that question. The figure shows that, neglecting the surface, which of course dries fairly quickly in the Southern U.S. in the absence of rain, the moisture state at the 20-cm depth drops to about 20%–30% of available capacity by Day 11 for both of the soils with finer textures. In fact, this level is considered to be a rather conservative threshold under which maize may start to experience stress by some authors [54,55]. However, the moisture level never drops to that state for any other depths during the irrigation cycle. Taking all evidence into account, it appears that the POME model trod a fine line between efficiency and stress, particularly for the finer soil classes. However, even these soils did not become stressed until the very end of the cycle, and it is not known what the impacts of this small stress would be on the final yield. A good percentage of the root mass for mature maize plants resides around the 20-cm depth, though, so if this stress level

were to be maintained for some time, it would undoubtedly affect yields. How long this stress would be maintained would depend on conditions that prevailed subsequent to this irrigation cycle.

In conclusion, this study has demonstrated the utility of the POME model to aid in irrigation scheduling. The POME generated profiles were shown to be good approximations of those actually observed at a site very near the test field and to represent profiles generated from a complex mathematical model with overall errors less than 10%. When applied to irrigation, it led to a very efficient strategy, although perhaps overly efficient for finer soils with a high percentage of clay content. This is an issue that should be investigated further.

Acknowledgments

The authors would like to express their sincere gratitude to the anonymous reviewers for their constructive comments towards the improvment of this manuspricpt. This research was supported under the joint NSF/USDA Project "F/USDA/NIFA Type 2—Collaborative Research—Migration of Agricultural Production Back to the Southeast". The support of the project PI, Richard McNider, is appreciated.

Author Contributions

Mishra: overall concept, model development, coding, error analysis, manuscript draft. Ellenburg: GIS display, ET development, manuscript editing. Al-Hamdan: model development, concept consultation. Bruce: overall concept development, ET development. Cruise: overall concept; team supervision; manuscript editing. All authors have read and approved the final manuscript.

Appendix

The semi-empirical root water extraction term can be expressed as:

$$S(t) = \alpha S_{max}(t); \quad \alpha \leq 1 \tag{A1}$$

where *S(t)* is root uptake at time t, α is the soil water availability factor and S_{max} is the maximum potential uptake that is equivalent to the potential transpiration allowed by prevailing atmospheric conditions. The soil water availability factor α is computed as a function of pressure head following Feddes *et al.*'s [47] formulation (see Yadav *et al.* [45]):

$$\alpha(h) = \begin{cases} 0, & h \geq h_1 or h \leq h_4 \\ \frac{h-h_1}{h_2-H_1}, & h_2 \leq h \leq h_1 \\ 1, & h_3 \leq h \leq h_2 \\ \frac{h_4-h}{h_4-h_3}, & h_4 \leq h \leq h_3 \end{cases} \tag{A2}$$

The values of limiting pressure heads were obtained from Veenhof and McBride [56] as follows: $\psi_1 = -15$ cm, $\psi_4 = -15{,}000$ cm. The van Genuchten [57] model is used to relate the effective saturation to pressure head:

$$\theta_e = \begin{cases} \theta_s, & h \geq 0 \\ 1/[1 + |\sigma h|^{\omega}]^{\beta}, & h < 0 \end{cases} \tag{A3}$$

where θ_e is the effective saturation ranging from 1–0, θ_s is the saturated moisture content, θ_r is the residual moisture content and h is the pressure head at the current moisture content. σ, ω and β are curve fitting parameters. These soil-dependent parameters were calibrated to the individual soils used in this study.

Evapotranspiration is estimated using the FAO-Penman two-stage approach, partitioning between surface evaporation and crop transpiration [2].

After the volume of water uptake by the roots is computed, a root distribution function is used to distribute the moisture uptake throughout the root zone. Smax is calculated assuming that the water uptake is proportional to the root density [58] and is formulated in a similar fashion to that of Yadav *et al.* [45] as:

$$S_{max}(Z,t) = \frac{L_{nrd}(Z_r)T_p(t)}{L_r(t)} \tag{A4}$$

where L_r is the total root depth, a function of the growth stage of the crop, Z_r is the normalized root depth ($Z_r = Z/L_r$) and L_nrd is the normalized root density distribution given by Wu *et al.* [52] and expressed as:

$$L_{nrd}(Z_r) = R_0 + R_1 Z_r + R_2(Z_r)^2 + R_3(Z_r)^3 \tag{A5}$$

where R_n (n = 0, 1, 2, 3) are crop-specific coefficients. The crop-specific coefficients were obtained from Wu *et al.* [52] from root distribution data attributed to Upchurch and Ritchie [59] and Merrill *et al.* [60] and are as follows: R_0 = 2.15, R_1 = −1.67, R_2 = −2.36 and R_3 = 1.88.

In addition to the limiting soil water availability factor, a root compensating index (φ) [61] as a function of both the root density distribution, as well as the soil moisture availability is included, such that:

$$\varphi(z,h,t) = \frac{\alpha F^{\lambda}}{\sum \alpha F^{\lambda}} \tag{A6}$$

for each layer, where F is a root distribution function and λ is a crop-specific coefficient. This additional index allows water stress in one part of the root zone to be compensated for by other moisture root zone layers. Combining both the soil availability factor with the root compensating factor, Yadav *et al.* [45] presented the following equation using the root density distribution function of Wu *et al.* [52]:

$$S(z,h,t) = \frac{\alpha^2(h)[L_{nrd}(Z_r)]^{\lambda}}{\Delta z \sum_0^{L_r} \alpha(h)[L_{nrd}(Z_r)]^{\lambda}} T_p(t) \tag{A7}$$

S(z,h,t) was used to simulate the root water uptake in this model. The crop-specific coefficient (λ) was optimized based on optimal moisture content, so that it best fit Equation (A4) and hovered around a value of one.

To simulate drainage, water is allowed to move vertically in each soil layer modeled if the water content is above field capacity and the layer below is below saturation. The amount of water that moves from one layer to the next is calculated on the storage routing methodology of the Soil Water and Assessment Tool (SWAT, [46]):

$$w = \theta_{excess} * [1 - e^{\frac{-\delta t}{TT_{perc}}}] \tag{A8}$$

where, for each layer, w is the amount of water drained, θ_{excess} is the amount of drainable water, $-\delta t$ is the length of the time step in hours and TT_{perc} is the travel time for drainage. TT_{perc} is defined as the

difference between the saturated (θ_{SAT}) and field capacity (θ_{FC}) moisture states divided by the hydraulic conductivity (K_{SAT}):

$$TT_{perc} = \frac{\theta_{SAT} - \theta_{FC}}{K_{SAT}} \tag{A9}$$

Conflicts of Interest

The authors declare no conflict of interest.

References

1. Burt, C.; Clemmens, A.; Strelkoff, T.; Solomon, K.; Bliesner, R.; Hardy, L.; Howell, T.; Eisenhauer, D. Irrigation Performance Measures: Efficiency and Uniformity. *J. Irrig. Drain. Eng.* **1997**, *123*, 423–442.
2. Allen, R.G.; Pereira, L.S.; Raes, D.; Smith, M. *Crop Evapotranspiration—Guidelines for Computing Crop Water Requirements—FAO Irrigation and Drainage Paper 56*; FAO: Rome, Italy, 1998; Volume 300, p. 6541.
3. Fereres, E.; Connor, D. Sustainable water management in agriculture. In *Challenges of the New Water Policies for the XXI Century*, Proceedings of the Seminar on Challenges of the New Water Policies for the 21st Century, Valencia, Spain, 29–31 October 2002; p. 164.
4. Ozdogan, M.; Gutman, G. A new methodology to map irrigated areas using multi-temporal MODIS and ancillary data: An application example in the continental US. *Remote Sens. Environ.* **2008**, *112*, 3520–3537.
5. Schaible, G.D.; Aillery, M.P. *Water Conservation in Irrigated Agriculture: Trends and Challenges in the Face of Emerging Demands*; US Department of Agriculture, Economic Research Service: Washington, DC, USA, 2012.
6. Kenny, J.F.; Barber, N.L.; Hutson, S.S.; Linsey, K.S.; Lovelace, J.K.; Maupin, M.A. *Estimated Use of Water in the United States in 2005*; US Geological Survey: Reston, VA, USA, 2009.
7. Fereres, E.; Soriano, M.A. Deficit irrigation for reducing agricultural water use. *J. Exp. Bot.* **2007**, *58*, 147–159.
8. Zhang, H.; Oweis, T.Y.; Garabet, S.; Pala, M. Water-use efficiency and transpiration efficiency of wheat under rain-fed conditions and supplemental irrigation in a Mediterranean-type environment. *Plant Soil* **1998**, *201*, 295–305.
9. Sammis, T.; Sharma, P.; Shukla, M.; Wang, J.; Miller, D. A water-balance drip-irrigation scheduling model. *Agric. Water Manag.* **2012**, *113*, 30–37.
10. Starks, P.J.; Heathman, G.C.; Ahuja, L.R.; Ma, L. Use of limited soil property data and modeling to estimate root zone soil water content. *J. Hydrol.* **2003**, *272*, 131–147.
11. Scott, C.A.; Bastiaanssen, W.G.M.; Ahmad, M.U.D. Mapping Root Zone Soil Moisture Using Remotely Sensed Optical Imagery. *J. Irrig. Drain. Eng.* **2003**, *129*, 326–335.
12. Kondratyev, K.Y.; Melentyev, V.V.; Rabinovich, Y.I.; Shulgina, E.M. Passive Microwave Remote Sensing of Soil Moisture. In Proceedings of the 11th International Symposium on Remote Sensing Environment, University of Michigan, Ann Arbor, MI, USA, 25–29 April 1977.

13. Arya, L.M.; Richter, J.C.; Paris, J.F. Estimating profile water storage from surface zone soil moisture measurements under bare field conditions. *Water Resour. Res.* **1983**, *19*, 403–412.
14. Srivastava, S.; Yograjan, N.; Jayaraman, V.; Rao, P.; Chandrasekhar, M. On the relationship between ERS-1 SAR/backscatter and surface/sub-surface soil moisture variations in vertisols. *Acta Astronaut.* **1997**, *40*, 693–699.
15. Kostov, K.G.; Jackson, T.J. Estimating profile soil moisture from surface-layer measurements: A review. *Proc. SPIE* **1993**,*1941* pp. 125–136.
16. Jackson, T.J. Profile soil moisture from surface measurements. *J. Irrig. Drain. Div. Am. Soc. Civil Eng.* **1980**, *106*, 81–92.
17. Reutov, E.; Shutko, A. Prior-knowledge based- soil moisture determination by microwave radiometry. *Soviet J. Remote Sens.* **1986**, *5*, 100–125.
18. Singh, V. *Hydrologic Systems: Watershed Modeling*; Prentice Hall: Englewood, NJ, USA, 1988; Volume 2.
19. De Troch, F.; Troch, P.; Su, Z.; Lin, D. Application of remote sensing for hydrological modelling. In *Distributed Hydrological Modelling*; Springer: Dordrecht, The Netherlands, 1996; pp. 165–191.
20. Assouline, S.; Tessier, D.; Bruand, A. A conceptual model of the soil water retention curve. *Water Resour. Res.* **1998**, *34*, 223–231.
21. Pachepsky, Y.; Guber, A.; Jacques, D.; Simunek, J.; Van Genuchten, M.T.; Nicholson, T.; Cady, R. Information content and complexity of simulated soil water fluxes. *Geoderma* **2006**, *134*, 253–266.
22. Al-Hamdan, O.Z.; Cruise, J.F. Soil Moisture Profile Development from Surface Observations by Principle of Maximum Entropy. *J. Hydrol. Eng.* **2010**, *15*, 327–337.
23. Koekkoek, E.; Booltink, H. Neural network models to predict soil water retention. *Eur. J. Soil Sci.* **1999**, *50*, 489–495.
24. Kornelsen, K.C.; Coulibaly, P. Root-zone soil moisture estimation using data-driven methods. *Water Resour. Res.* **2014**, *50*, 2946–2962.
25. Huang, C.; Li, X.; Lu, L.; Gu, J. Experiments of one-dimensional soil moisture assimilation system based on ensemble Kalman filter. *Remote Sens. Environ.* **2008**, *112*, 888–900.
26. Moore, R.J. The probability-distributed principle and runoff production at point and basin scales. *Hydrol. Sci. J.* **1985**, *30*, 273–297.
27. Mays, D.C.; Faybishenko, B.A.; Finsterle, S. Information entropy to measure temporal and spatial complexity of unsaturated flow in heterogeneous media. *Water Resour. Res.* **2002**, *38*, 49.1–49.11.
28. Singh, V.P. Entropy theory for derivation of infiltration equations. *Water Resour. Res.* **2010**, *46*, doi:10.1029/2009WR008193.
29. Pan, F.; Pachepsky, Y.A.; Guber, A.K.; Hill, R.L. Information and complexity measures applied to observed and simulated soil moisture time series. *Hydrol. Sci. J.* **2011**, *56*, 1027–1039.
30. Mishra, V.; Cruise, J.F.; Mecikalski, J.R.; Hain, C.R.; Anderson, M.C. A remote-sensing driven tool for estimating crop stress and yields. *Remote Sens.* **2013**, *5*, 3331–3356.
31. Bras, R.L. *Hydrology: An Introduction to Hydrologic Science*; Addison-Wesley: Reading, MA, USA, 1990.
32. Singh, V.P. *Elementary Hydrology*; Pearson College Division: Engelwood Cliffs, NJ, USA, 1992.

33. Clapp, R.B.; Hornberger, G.M. Empirical equations for some soil hydraulic properties. *Water Resour. Res.* **1978**, *14*, 601–604.
34. Heber Green, W.; Ampt, G.A. Studies on Soil Phyics. *J. Agric. Sci.* **1911**, *4*, 1–24.
35. Kostiakov, A.N. On the dynamics of the coefficient of water-percolation in soils and on the necessity for studying it from a dynamic point of view for purposes of amelioration. In Proceedings of the Transactions of 6th Congress of International Soil Science Society, Moscow, Russia, 1932; pp. 17–21.
36. Horton, R.E. The Interpretation and Application of Runoff Plat Experiments with Reference to Soil Erosion Problems. *Soil Sci. Soc. Am. J.* **1939**, *3*, 340.
37. Holtan, H. *A Concept for Infiltration Estimates in Watershed Engineering*; USDA-ARS Bulletin 41-51: Washington, DC, USA, 1961.
38. Singh, V. The use of entropy in hydrology and water resources. *Hydrol. Process.* **1997**, *11*, 587–626.
39. Shannon, C.E. A Mathematical Theory of Communication. *Bell Syst. Tech. J.* **1948**, *27*, 379–423.
40. Jaynes, E.T. Information theory and statistical mechanics-1. *Phys. Rev.* **1957**, *106*, 620–630.
41. Jaynes, E.T. Information Theory and Statistical Mechanics-II. *Phys. Rev.* **1957**, *108*, 171–190.
42. Barbe, D.E.; Cruise, J.F.; Singh, V.P. Solution of Three Constraint Entropy Based Velocity Distribution. *J. Hydraul. Eng.* **1991**, *117*, 1389–1396.
43. Singh, V.P. Hydrologic synthesis using entropy theory: Review. *J. Hydrol. Eng.* **2011**, *16*, 421–433.
44. Chiu, C.L. Entropy and Probability Concepts in Hydraulics. *J. Hydraul. Eng.* **1987**, *113*, 583–599.
45. Yadav, B.K.; Mathur, S.; Siebel, M.A. Soil moisture dynamics modeling considering the root compensation mechanism for water uptake by plants. *J. Hydrol. Eng.* **2009**, *14*, 913–922.
46. Neitsch, S.L.; Arnold, J.G.; Kiniry, J.R.; Williams, J.R. *SWAT Theoretical Documentation Version 2009*; Technical Report Technical Report No. 406; Texas Water Resources Institute: College Station, TX, USA, 2011.
47. Feddes, R.A.; Kowalik, P.J.; Zaradny, H.; others. *Simulation of Field Water Use and Crop Yield*; Centre for Agricultural Publishing and Documentation: Wageningen, The Netherlands, 1978.
48. Paudel, K.P.; Limaye, A.S.; Hatch, L.U.; Cruise, J.F.; Musleh, F. Development of an optimal water allocation decision tool for the major crops during the water deficit period in the southeast United States. *Nat. Resour. Model.* **2005**, *18*, 281–306.
49. Nash, J.; Sutcliffe, J. River flow forecasting through conceptual models part I—A discussion of principles. *J. Hydrol.* **1970**, *10*, 282–290.
50. ASCE Task Committee Defination of Criteria for Evaluation of Watershed Models. *J. Irrig. Drain. Eng.* **1993**, *119*, 429–442.
51. Poulovassilis, A.; Anadranistakis, M.; Liakatas, A.; Alexandris, S.; Kerkides, P. Semi-empirical approach for estimating actual evapotranspiration in Greece. *Agric. Water Manag.* **2001**, *51*, 143–152.
52. Wu, J.; Zhang, R.; Gui, S. Modeling soil water movement with water uptake by roots. *Plant Soil* **1999**, *215*, 7–17.
53. Çakir, R. Effect of water stress at different development stages on vegetative and reproductive growth of corn. *Field Crops Res.* **2004**, *89*, 1–16.

54. Luo, Y.; He, C.; Sophocleous, M.; Yin, Z.; Hongrui, R.; Ouyang, Z. Assessment of crop growth and soil water modules in SWAT2000 using extensive field experiment data in an irrigation district of the Yellow River Basin. *J. Hydrol.* **2008**, *352*, 139–156.
55. Taylor, T.; Ravet, F. *A Meteorologically Driven Maize Stress Indicator Model*; AgRISTARS EW/CCA Rep. EW-U1-04119, JSC-17399; Lyndon B. Johnson Space Center: Houston, TX, USA, 1981.
56. Veenhof, D.; McBride, R. A preliminary performance evaluation of a soil water balance model (SWATRE) on corn producing croplands in the RM of Haldimand-Norfolk. In *Soil Compaction Susceptibility and Compaction Risk Assessment for Corn Production*; Centre for Land and Biological Resources Research AAFC: Ottawa, ON, USA, 1994; pp. 112–142.
57. Van Genuchten, M.T. A closed-form equation for predicting the hydraulic conductivity of unsaturated soils. *Soil Sci. Soc. Am. J.* **1980**, *44*, 892–898.
58. Perrochet, P. Water uptake by plant roots—A simulation model, I. Conceptual model. *J. Hydrol.* **1987**, *95*, 55–61.
59. Upchurch, D.; Ritchie, J. Battery-operated color video camera for root observations in mini-rhizotrons. *Agron. J.* **1984**, *76*, 1015–1017.
60. Merrill, S.; Doering, E.; Reichman, G. Application of a minirhizotron with flexible, pressurized walls to a study of corn root growth. In *Minirhizotron Observation Tubes: Methods and Applications for Measuring Rhizosphere Dynamics*; American Society of Agronomy: Madison, WI, USA, 1987; pp. 131–143.
61. Li, K.; De Jong, R.; Boisvert, J. An exponential root-water-uptake model with water stress compensation. *J. Hydrol.* **2001**, *252*, 189–204.